Bandwidth shaping of microresonator-based frequency combs via dispersion engineering

Yoshitomo Okawachi,[1,*] Michael R. E. Lamont,[1,2] Kevin Luke,[3] Daniel O. Carvalho,[3] Mengjie Yu,[1] Michal Lipson,[2,3] and Alexander L. Gaeta[1,2]

[1]*School of Applied and Engineering Physics, Cornell University, Ithaca, New York 14853, USA*

[2]*Kavli Institute at Cornell for Nanoscale Science, Ithaca, New York 14853, USA*

[3]*School of Electrical and Computer Engineering, Cornell University, Ithaca, New York 14853, USA*

**Corresponding author: yo22@cornell.edu*

Received April 8, 2014; revised May 9, 2014; accepted May 9, 2014;
posted May 13, 2014 (Doc. ID 209756); published June 9, 2014

We investigate experimentally and theoretically the role of group-velocity dispersion and higher-order dispersion on the bandwidth of microresonator-based parametric frequency combs. We show that the comb bandwidth and the power contained in the comb can be tailored for a particular application. Additionally, our results demonstrate that fourth-order dispersion plays a critical role in determining the spectral bandwidth for comb bandwidths on the order of an octave. © 2014 Optical Society of America

OCIS codes: (140.3948) Microcavity devices; (190.4380) Nonlinear optics, four-wave mixing; (190.4390) Nonlinear optics, integrated optics.
http://dx.doi.org/10.1364/OL.39.003535

Four-wave mixing (FWM) parametric oscillation in high-Q microresonators is a highly effective approach for producing optical frequency combs [1–7]. Since the parametric frequency comb bandwidth is determined by phase-matching contributions from linear and nonlinear effects, broadband and narrowband combs require different operating conditions. A bandwidth regime of importance is that associated with the generation of octave-spanning combs [3,4], which are critical for applications in spectroscopy, precision frequency metrology, and optical clocks. Alternatively, such combs can be used as a chip-scale, multiple-wavelength source for wavelength-division multiplexing (WDM) systems [8–10]. For such an application, efficient power consumption is critical, and the comb bandwidth should be restricted to the operation regime of the particular WDM system.

In this Letter, we theoretically and experimentally investigate the role of group-velocity dispersion (GVD) and higher-order dispersion on the bandwidth of silicon–nitride-based parametric frequency combs. We show that dispersion engineering in the silicon–nitride (Si_3N_4) platform allows for control of the comb bandwidth and power in the comb to adapt to a particular application.

We use a theoretical model based on a modified Lugiato–Lefever equation (LLE) to fully simulate the dynamics of comb generation in Si_3N_4 microring resonators [11–19]. The modified LLE describes the propagation of the intracavity field $E(t,\tau)$ in the microring and is written as,

$$t_R\frac{\partial E(t,\tau)}{\partial t}=\left[-\alpha-i\delta_0+iL\sum_{n\geq 2}\frac{\beta_n}{n!}\left(i\frac{\partial}{\partial\tau}\right)^n+i\gamma L\left(1+\frac{i}{\omega_0}\frac{\partial}{\partial\tau}\right)|E(t,\tau)|^2\right]E(t,\tau)+\sqrt{\theta}E_{\mathrm{in}},\quad(1)$$

where t_R is the round trip time in the resonator, α is the total round trip loss, δ_0 is the phase detuning between the cavity resonance and the pump frequencies, θ is the transmission coefficient between the resonator and the bus waveguide, L is the cavity length, γ is the nonlinear parameter, ω_0 is the angular frequency of the pump, and β_k corresponds to the kth-order dispersion coefficients of the Taylor expansion of the propagation constant. Here, τ represents the temporal coordinate within the time scale of a single round trip and t represents the long-time-scale evolution over many round trips. Our modified LLE model, which includes higher-order dispersion and self-steepening, enables simulations of combs spanning an octave of bandwidth [16] and has shown excellent agreement with previous experimental demonstration. We investigate the effects of these terms on sideband generation from FWM by analyzing the coupled mode equations associated with the field $E(t,\tau)=A_0+A_++A_-$ [19–21], where A_0 is the pump field and A_+ and A_- represent the symmetrically detuned sidemodes. For our analysis, we assume that the amplitude of the sidebands are much smaller than A_0, in which case the coupled equations are given as

$$t_R\frac{\partial A_0}{\partial t}=-(\alpha+i\delta_0)A_0+i\gamma L|A_0|^2A_0+2i\gamma LA_0^*A_+A_-+\sqrt{\theta}E_{\mathrm{in}},\quad(2)$$

$$t_R\frac{\partial A_+}{\partial t}=-\left[\alpha+i\Delta\kappa+iL\sum_{n=3,5,\ldots}\frac{\beta_n}{n!}\Omega^n+2iL\frac{\Omega}{\omega_0}\gamma|A_0|^2\right]A_++i\gamma L\left(1-\frac{\Omega}{\omega_0}\right)A_0^2A_-^*,\quad(3)$$

$$t_R\frac{\partial A_-}{\partial t}=-\left[\alpha+i\Delta\kappa-iL\sum_{n=3,5,\ldots}\frac{\beta_n}{n!}\Omega^n-2iL\frac{\Omega}{\omega_0}\gamma|A_0|^2\right]A_-+i\gamma L\left(1+\frac{\Omega}{\omega_0}\right)A_0^2A_+^*,\quad(4)$$

where Ω is the sideband detuning, and the phase mismatch is given by

$$\Delta\kappa = \delta_0 - L\sum_{n=2,4,\ldots}\frac{\beta_n}{n!}\Omega^n - 2\gamma L|A_0|^2. \quad (5)$$

The resulting solutions for A_+ and A_- are

$$A_+(t) = A_+(0)\exp\left[\Lambda(\Omega)\frac{t}{t_R}\right] \times \exp\left[-i\left(L\sum_{n=3,5,\ldots}\frac{\beta_n}{n!}\Omega^n + 2\gamma L\frac{\Omega}{\omega_0}|A_0|^2\right)\frac{t}{t_R}\right], \quad (6)$$

$$A_-(t) = A_-(0)\exp\left[\Lambda(\Omega)\frac{t}{t_R}\right] \times \exp\left[i\left(L\sum_{n=3,5,\ldots}\frac{\beta_n}{n!}\Omega^n + 2\gamma L\frac{\Omega}{\omega_0}|A_0|^2\right)\frac{t}{t_R}\right], \quad (7)$$

where $\Lambda(\Omega) = -\alpha + \sqrt{[\gamma L(1-\Omega^2/\omega_0^2)|A_0|^2]^2 - (\Delta\kappa)^2}$ is the gain coefficient. The gain coefficient Λ and phase mismatch $\Delta\kappa$ depend on the even-orders of dispersion, while the odd-order dispersion terms add a phase contribution to the sidebands which is opposite in sign with respect to each other. The overall comb bandwidth is highly dependent on the initial sideband detuning. As the detuning increases, contributions from higher-order terms become most important and must be taken into account in the analysis. While the odd-order terms do not contribute directly to the amplitude growth, these phase terms are relevant for pulse shaping and modelocking. The inclusion of the self-steepening term does not affect $\Delta\kappa$, but modifies the nonlinear term in the gain and contributes an additional phase term.

We theoretically investigate how the comb bandwidth can be controlled using two different waveguide cross sections of 690×1900 nm and 910×1800 nm. Previously, the high stress in silicon–nitride films prevented deposition of high quality nitride films, which in turn limited the magnitude of the anomalous GVD that could be reached. However, recent advances in fabrication techniques have allowed for deposition of thick, high-quality films [22], enabling higher anomalous GVD values and access to a wider parameter space for waveguide dispersion. The GVD for the Si_3N_4 waveguide is shown in Fig. 1(a) which was calculated with a finite-element mode-solver. For cross sections where waveguide dispersion dominates over material dispersion, the taller waveguide height results in a larger anomalous GVD. For the comb simulations, the microring has a 100 μm radius and is pumped at 1550 nm. The resonator is in the undercoupled regime, with 50% power transmission. The power in the coupling waveguide is 650 and 400 mW for the 690×1900 nm and 910×1800 nm cross sections, respectively. Figure 1(b) shows the simulated comb spectra for the two different dimensions. While the region of anomalous GVD for the 690×1900 nm cross section spans only 550 nm, the low anomalous GVD at the pump wavelength allows the comb to span a bandwidth far exceeding the anomalous GVD region. In contrast, for the 910×1800 nm cross section, for which the anomalous

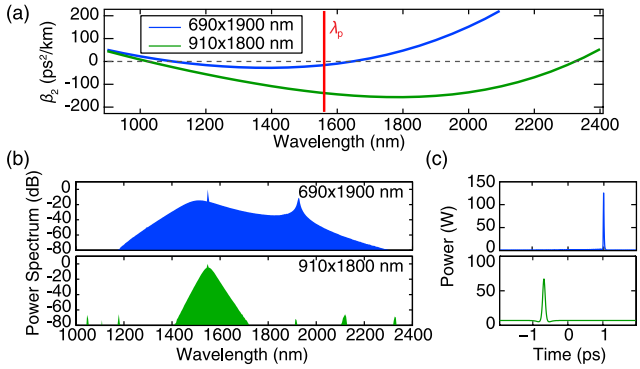

Fig. 1. (a) Simulated GVD for silicon–nitride waveguides with cross sections 690×1900 nm (blue) and 910×1800 nm (green). (b) Simulated comb spectra and (c) temporal plot for 260 GHz free spectral range (FSR) Si_3N_4 microring resonators with cross sections 690×1900 nm (top) and 910×1800 nm (bottom).

GVD region spans 1250 nm, the large anomalous GVD at the pump wavelength results in narrowband comb generation. For our simulated parameters, self-steepening has a minimal effect on the generated comb bandwidth. Considering the phase mismatch equation with only the GVD contribution, the detuning is inversely proportional to the square root of β_2. This implies that for larger (smaller) β_2 values the smaller (larger) the frequency detuning results in a narrower (broader) bandwidth. The bandwidth dependence on GVD is consistent with the predictions based on steady-state analysis by Coen and Erkintalo [15]. Figure 1(c) shows the temporal profile of the simulated combs and indicates single-pulse modelocking and cavity soliton formation, which is indicative of a stabilized comb [6,7]. The narrower bandwidth allows for a higher power per comb line, allowing for more efficient power conversion from the pump to the comb lines, which is critical for an energy-efficient multiple-wavelength source for WDM applications.

Next, we investigate the effects of higher-order dispersion by modeling comb generation at three different pump wavelengths, 1550, 1400, and 1200 nm. Figure 2(a) shows the GVD and fourth-order dispersion (FOD) for a 690×1900 nm cross section, and Fig. 2(b) shows the simulated comb spectra for each pump wave-

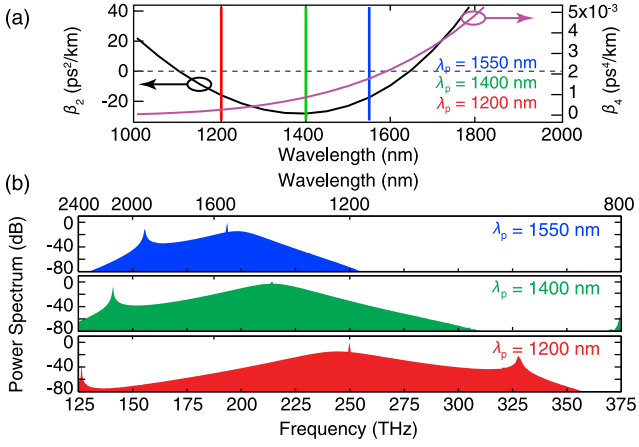

Fig. 2. (a) Simulated GVD and FOD for 690×1900 nm cross section Si_3N_4 waveguide. (b) Simulated comb spectra for pump wavelengths of 1550, 1400, and 1200 nm.

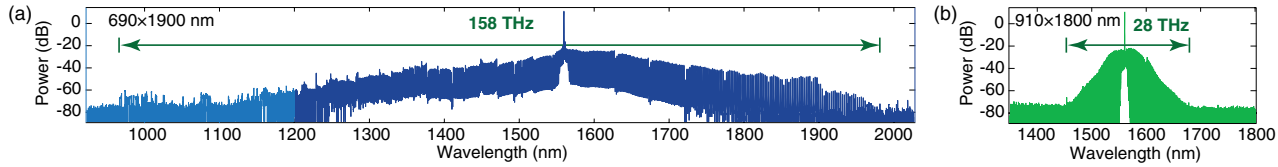

Fig. 3. Measured comb spectra in Si_3N_4 microrings with cross sections (a) 690×1900 nm and (b) 910×1800 nm.

length. In each case, a stabilized, single-pulsed modelocked comb is achieved. In comparing the comb spectra for the 1550 and 1400 nm pumps, the comb bandwidth is significantly broader for the 1400 nm pump even though the magnitude of GVD is smaller for the 1550 nm pump. This is due to the FOD contribution to phase matching, which becomes significant for FWM over broader bandwidths. The broadest comb is generated with the 1200 nm pump, where the GVD and FOD values are the lowest. While the GVD at 1200 nm ($\beta_2 = -16$ ps^2/km) is close to that at 1550 nm ($\beta_2 = -17$ ps^2/km), as a result of the different FOD values at 1200 nm ($\beta_4 = 2.6 \times 10^{-4}$ ps^4/km) and 1500 nm ($\beta_4 = 1.8 \times 10^{-3}$ ps^4/km), the 30 dB bandwidth with a 1200 nm pump is 1.8 times broader than that with a 1550 nm pump. Our results show that, while low anomalous GVD is a necessary requirement for broadband combs, small FOD is also critical to further extend the bandwidth.

In addition, we observe dispersive wave (DW) formation at the edges of the comb spectra. Recent studies have investigated the role of third-order dispersion (TOD) and FOD on DW formation [15,17]. Since the dispersion profile has two zero-GVD (ZGVD) points at 1100 and 1646 nm, we observe in Fig. 2(b), on the long wavelength side, the DW redshifts as expected as the pump wavelength is tuned to shorter wavelengths away from the long-λ ZGVD point. Furthermore, at the short wavelength side, a second DW redshifts as the pump wavelength is tuned toward the short-λ ZGVD point. The wavelength for DW formation can be predicted by phase-matching conditions between the cavity soliton and the DW wave across a ZGVD point [23]. While TOD and FOD contribute to DW generation, due to the broad bandwidth of the generated comb, these contributions alone do not accurately predict the spectral positions for DW generation and the group velocity of the soliton and the DW, and higher-order dispersion terms must be taken into account.

We investigate the predictions from Fig. 1 experimentally by pumping at a microring resonance near 1560 nm using an amplified single-frequency laser. The power in the coupling waveguide is 650 mW. To cover the entire spectral measurement range, we utilize two optical spectrum analyzers operating from 900 to 1200 nm and from 1200 to 2400 nm. Figures 3(a) and 3(b) show the measured spectra from the 690×1900 nm and 910×1800 nm cross section microring, respectively. Each generated comb undergoes a transition to the low-noise state characteristic of modelocking as observed in previous studies [4,6]. The 690×1900 nm microring [Fig. 3(a)] generates a 158 THz bandwidth comb, which represents the broadest comb generated to date in a silicon–nitride platform. In contrast, the comb generated in the 690×1900 nm microring [Fig. 3(a)] spans a significantly narrower bandwidth of 28 THz. The measured spectra are in good agreement with our theoretical predictions [Fig. 1(b)]. The difference in bandwidth can arise from discrepancies in estimates of the losses and the wavelength-dependent coupling conditions for the resonator and from deviations in dispersion resulting from fabrication tolerances.

We further investigate narrowband comb generation. Figure 4(a) shows the GVD for a 950×1700 nm cross section Si_3N_4 microring with two different radii of 100 and 46 μm, which corresponds to free spectral ranges (FSRs) of 260 and 530 GHz, respectively. The mode-solver takes into account the radius of curvature of the microring, which results in a small deviation in the GVD from that of a straight waveguide. Figures 4(b) and 4(c) show the simulated comb spectra for the two different FSRs. The taller waveguide further increases the anomalous GVD, narrowing the comb bandwidth. The spectra show 16 and 8 combs lines over a 3 dB bandwidth for the 260 and 530 GHz FSR resonators, respectively. The comb bandwidth is primarily dictated by the microring GVD, and the spacing is determined by the cavity FSR. Simulations indicate that by adjusting the coupling between the microring and the bus waveguide, power conversion of the pump to the comb lines as high as 60% can be achieved. Thus, the microring dispersion and FSR can be controlled such that the comb-based multiple wavelength source is customized to the WDM system.

In conclusion, we investigate the role of GVD and higher-order dispersion on parametric comb generation. The flexibility in the Si_3N_4 platform allows for independent control of the dispersion and FSR offering potential for use as a power-efficient multiple-wavelength source in a WDM system. In addition, we observe that FOD plays a large role for comb bandwidths of the order of an octave and hence, the waveguide geometry must be precisely engineered based on the bandwidth requirements for comb generation.

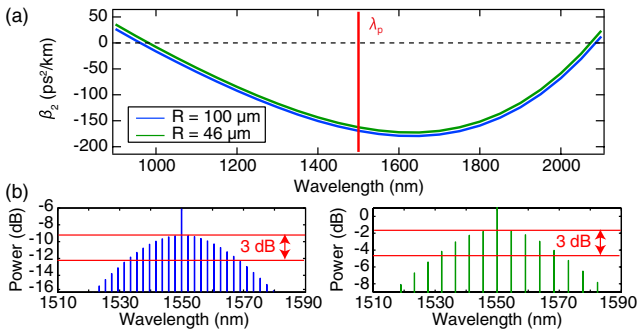

Fig. 4. (a) Simulated GVD for 950×1400 nm cross section Si_3N_4 microrings for a 100 and 46 μm radius. (b) Simulated comb spectra in 100 and 46 μm radius microrings, corresponding to 260 and 530 GHz FSRs, respectively.

We acknowledge support from the Defense Advanced Research Projects Agency via the QuASAR program, the Air Force Office of Scientific Research under Grant FA9550-12-1-0377 and Semiconductor Research Corporation. This work was performed in part at the Cornell Nano-Scale Facility, a member of the National Nanotechnology Infrastructure Network, which is supported by the National Science Foundation (Grant ECS-0335765). We thank Y. H. Wen for useful discussions.

References

1. T. J. Kippenberg, R. Holzwarth, and S. A. Diddams, Science **332**, 555 (2011).
2. W. Liang, A. A. Savchenkov, A. B. Matsko, V. S. Ilchenko, D. Seidel, and L. Maleki, Opt. Lett. **36**, 2290 (2011).
3. P. Del'Haye, T. Herr, E. Gavartin, M. L. Gorodetsky, R. Holzwarth, and T. J. Kippenberg, Phys. Rev. Lett. **107**, 063901 (2011).
4. Y. Okawachi, K. Saha, J. S. Levy, Y. H. Wen, M. Lipson, and A. L. Gaeta, Opt. Lett. **36**, 3398 (2011).
5. S. B. Papp and S. A. Diddams, Phys. Rev. A **84**, 053833 (2011).
6. K. Saha, Y. Okawachi, B. Shim, J. S. Levy, R. Salem, A. R. Johnson, M. A. Foster, M. R. Lamont, M. Lipson, and A. L. Gaeta, Opt. Express **21**, 1335 (2013).
7. T. Herr, V. Brasch, J. D. Jost, C. Y. Wang, N. M. Kondratiev, M. L. Gorodetsky, and T. J. Kippenberg, Nat. Photonics **8**, 145 (2014).
8. J. S. Levy, K. Saha, Y. Okawachi, M. A. Foster, M. Lipson, and A. L. Gaeta, IEEE Photon. Technol. Lett. **24**, 1375 (2012).
9. P.-H. Wang, F. Ferdous, H. Miao, J. Wang, D. E. Leaird, K. Srinivasan, L. Chen, V. Aksyuk, and A. M. Weiner, Opt. Express **20**, 29284 (2012).
10. J. Pfeifle, V. Brasch, M. Lauermann, Y. Yu, D. Wegner, T. Herr, K. Hartinger, P. Schindler, J. Li, D. Hillerkuss, R. Schmogrow, C. Weimann, R. Holzwarth, W. Freude, J. L euthold, T. J. Kippenberg, and C. Koos, Nat. Photonics **8**, 375 (2014).
11. L. A. Lugiato and R. Lefever, Phys. Rev. Lett. **58**, 2209 (1987).
12. M. Haelterman, S. Trillo, and S. Wabnitz, Opt. Commun. **91**, 401 (1992).
13. A. B. Matsko, A. A. Savchenkov, W. Liang, V. S. IlChenko, D. Seidel, and L. Maleki, Opt. Lett. **36**, 2845 (2011).
14. Y. K. Chembo and C. R. Menyuk, Phys. Rev. A **87**, 053852 (2013).
15. S. Coen and M. Erkintalo, Opt. Lett. **38**, 1790 (2013).
16. M. R. E. Lamont, Y. Okawachi, and A. L. Gaeta, Opt. Lett. **38**, 3478 (2013).
17. S. Wang, H. Guo, X. Bai, and X. Zeng, Opt. Lett. **39**, 2880 (2014).
18. L. Zhang, C. Bao, V. Singh, J. Mu, C. Yang, A. M. Agarwal, L. C. Kimerling, and J. Michel, Opt. Lett. **38**, 5122 (2013).
19. V. Torres-Company, D. Castelló-Lurbe, and E. Silvestre, Opt. Express **22**, 4678 (2014).
20. M. Haelterman, S. Trillo, and S. Wabnitz, Opt. Lett. **17**, 745 (1992).
21. T. Hansson, D. Modotto, and S. Wabnitz, Phys. Rev. A **88**, 023819 (2013).
22. K. Luke, A. Dutt, C. B. Poitras, and M. Lipson, Opt. Express **21**, 22829 (2013).
23. M. A. Foster, A. C. Turner, M. Lipson, and A. L. Gaeta, Opt. Express **16**, 1300 (2008).